Applied Physics B (2024) 130:165
https://doi.org/10.1007/s00340-024-08303-z

Applied Physics B
Lasers and Optics

RESEARCH

External-cavity tunable yellow-red laser based on Ng-cut KGW Raman conversion and frequency mixing

Yongpeng Yan[1,2] · Yuxiang Sun[1,2] · Xuezong Yang[2] · Chengjie Zhu[1,2] · Yan Feng[2]

Received: 5 July 2024 / Accepted: 7 August 2024 / Published online: 27 August 2024

Abstract
We demonstrated a wavelength discretely tunable laser with outputs at 572.6 nm, 589.1 nm, 603.8 nm, and 611.8 nm using external cavity Ng-cut KGW Raman conversion and intracavity frequency mixing. The multiple visible wavelengths were generated by utilizing this specially cut KGW crystal and the g[mm]g Raman configuration, as well as the temperature-dependent phase-matching characteristic of the LBO crystal. The maximum output powers at 572.6 nm, 589.1 nm, 603.8 nm, and 611.8 nm were measured to be 227 mW, 175 mW, 258 mW, and 103 mW respectively, with nearly fundamental Gaussian beam profiles. This work provides a monolithic setup capable of producing tunable yellow-red laser outputs through Raman and χ^2 frequency conversions for various applications such as air detection, optogenetics, biomedicine, and chemical analysis.

1 Introduction

Visible lasers play a crucial role in various fields including illumination and biological tissue imaging. Apart from the specific wavelength requirements, numerous applications necessitate wavelength-tunable capabilities for optimal performance, such as air detection, optogenetics, biomedicine, and chemical analysis [1–4]. Raman conversion, combined with a wavelength-tunable pump source (like a titanium-sapphire laser [5] or an optical fiber amplifier with a tunable filter [6]), is an effective technique to access these special lasers and can typically provide a tuning range of tens of nanometers. An alternative and affordable approach to emit diverse visible lasers within a single resonator is to exploit the multiple Raman frequency shifts [7] of anisotropy Raman crystals or adjust the phase matching conditions (temperature [8] or angle [9–11] of the nonlinear crystals) for various optical nonlinearities.

YVO_4 and KGW have been widely studied for efficient Raman conversion and abundant wavelength emission due to their mature growth technology and low processing cost. A lot of work regarding multiple visible wavelengths generation has been reported utilizing the YVO_4 crystal [7, 8, 12–15] cut at certain angles with the combination of temperature or angle tuning of the frequency-doubling crystals. Despite the rich emission bands of the aforementioned frequency-doubled YVO_4 Raman laser, the generated wavelengths are still relatively fixed as these lasers usually used an intracavity structure with a fixed pump wavelength stimulated by the rare-earth-doped gain media. KGW is also a good Raman crystal with favorable characteristics like notable gain, thermal conductivity, and damage threshold. To the best of our knowledge, the output power records of crystalline Raman lasers (except for the diamond) have all been generated in the KGW lasers [16, 17]. KGW is also one of the few reported crystals that can generate Stokes wavelength in an external-cavity architecture[18, 19], which provides a more flexible wavelength converge based on numerous pump selection. So far, the KGW crystals adopted in Raman lasers are usually Np-cut with the pump laser propagating along the Np-axis and polarization of the pump oriented at the Ng or Nm axes of the crystals. A prominent merit for such architectures is the simple and pure Raman frequency shift peak in Raman conversion, corresponding to 901 cm^{-1} in p[mm]p notion and 768 cm^{-1} in p[gg]p notion, respectively. Recently, a highly efficient yellow-orange KGW Raman laser was realized by aligning the polarization

✉ Yuxiang Sun
yx.sun.xy@hotmail.com

✉ Xuezong Yang
xuezong.yang@ucas.ac.cn

[1] Shanghai Institute of Optics and Fine Mechanics, Chinese Academy of Sciences, Shanghai 201800, China

[2] Hangzhou Institute for Advanced Study, University of Chinese Academy of Sciences, Hangzhou 310024, Zhejiang, China

of the pump source along the Ng- or Nm-axis of the crystal combining with intracavity frequency-doubling [9, 10]. As the KGW crystal is an anisotropic medium with promising Raman characteristics, it is anticipated that it could be utilized for versatile visible wavelength emissions when cut at specific orientations.

In this paper, a Ng-cut KGW crystal was used as the Raman medium in an external resonator. A 205 cm^{-1} Raman shift was observed in the spontaneous Raman spectrum along the Nm-axis. Consequently, in the g[mm]g configuration, multi-wavelength Stokes laser at 205 cm^{-1} shift was generated besides the primary shift of 901 cm^{-1}. When inserting a LBO crystal in the resonator and tuning its temperature for frequency-mixing of the fundamental and Stokes fields, a continuous-wave tunable yellow-red laser was realized with an output power at the level of hundred milliwatts.

2 Experimental setup

The schematic configuration is shown in Fig. 1a. A home-made linearly-polarized continuous-wave fiber amplifier centered at 1065.2 nm is utilized as the pump, providing a maximum power of 57 W. The full width at half maxima (FWHM) of the pump spectrum is approximately 16.3 GHz, which is significantly narrower than the Raman linewidth of KGW and thus offers a considerable gain coefficient [20]. A space isolator (SteadiBeam, AFR Ltd.) is placed after the pump to protect it against the backward beam. The pump polarization is adjusted using a half-wave plate (HWP). After being focused by a plano-convex lens (f = 75 mm), the pump beam enters the Raman resonator and converges at the center of the KGW crystal with a waist radius of 47 µm. The size of the pump waist is slightly larger than our previous work [21], aiming to match the Rayleigh range with the crystal length for the optimal utilization of pump power. The external Raman cavity is composed of two plano-concave mirrors with radius of curvature 50 mm (IC) and 100 mm (OC), respectively. To enhance the intracavity doubling efficiency, IC and OC are both coated highly reflective at 1178 nm (>99.9% R), and partially transmissive at 572 nm, 589 nm, 603 nm and 611 nm (78% T and 99.5% T for IC and OC, respectively). Besides, the OC is highly reflective at 1065 nm, which allows a pump double pass architecture. The reflectivity of the IC and OC at 1207 nm and 1238 nm is 99.85% and 99.8%, respectively. A 15×4×2 mm^3 Ng-cut KGW (manufactured by Castech Ltd.) is used as the Raman medium. The crystal structure is depicted in Fig. 1b, with the pump beam propagating along the Ng axis. This irregularly angle-cut KGW crystal exhibits more complex Raman scattering properties compared to the Np-cut crystals. To achieve a more diverse range of Raman peaks, we adjust the pump polarization along the Nm axis, and the spontaneous Raman spectrum (measured by HR Evolution & FLS980, Horiba Inc.) of the crystal in this direction is shown in Fig. 1c. The intensities have been normalized based on the main peak at 901 cm^{-1}. It can be observed that the 205 cm^{-1} peak reaches half the intensity of the main peak, indicating a significant gain coefficient. Thermal dissipation in KGW crystal is achieved by establishing contact with water-cooled copper at the bottom. A 10×4×4 mm^3 LBO crystal cut at $\theta = 90°$, $\phi = 0°$ (manufactured by Castech Ltd.) is inserted in the KGW cavity. The temperature of LBO is stabilized using a precise digital temperature control module (TCB-NE, Xiafan Tech Ltd.) with an adjustment accuracy of 0.1° C.

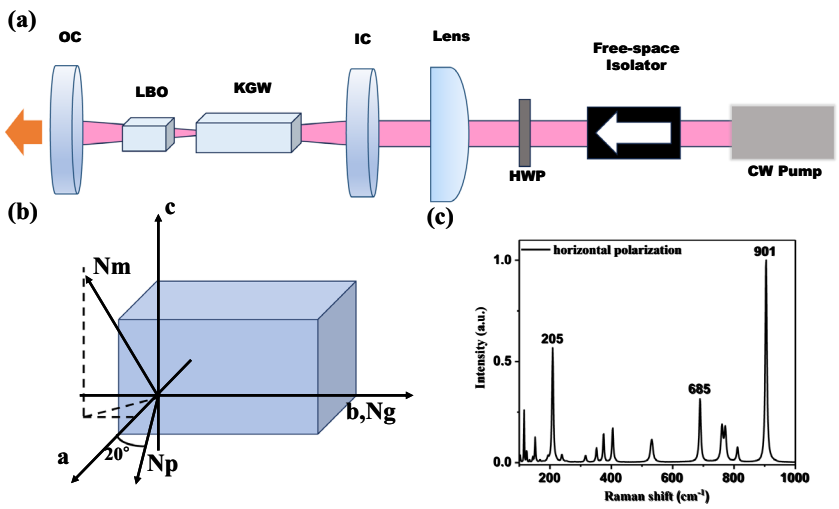

Fig. 1 **a** Schematic diagram of the intracavity frequency-doubling wavelength-tunable KGW Raman laser. **b** Ng-cut KGW crystal structure in the Cartesian coordinate system. **c** Spontaneous Raman spectra of KGW crystals along the Nm axis

3 Results and discussions

The resonator is first analyzed without the insertion of LBO and the double-ended output Stokes power is illustrated in Fig. 2. The output Stokes power increases linearly above the resonator threshold of 13.3 W until the pump power reaches 32.2 W, and the slope efficiency is 0.041%. Subsequently, the Stokes power elevated acceleratingly to 30.0 mW at the pump power of 40.2 W, followed by a 0.12% linear growth. An output power of 52 mW is obtained at the maximum pump power of 57 W. This low-efficiency output is not surprising since we use an extremely high-Q resonator at the Stokes wavelengths. The difference in the slope, however, suggests that the resonator underwent certain alterations as the pump power increased, which will be covered later.

To obtain a thorough knowledge of the scattering process caused by the pump laser inside the resonator, the Stokes spectrums (measured by AQ6370D, Yokogawa Inc.) are briefly characterized with output power elevating, shown in Fig. 3. The Stokes laser at 1178.3 nm is predominantly generated near the threshold, followed by the emergence of parasitic oscillation at 1207.5 nm. The frequency shift of these two wavelengths is consistent with 205 cm^{-1} peak shown in Fig. 1c. It is noteworthy that the power transfer of the pump to the 1178.3 nm laser is hindered at the emergence of the 1207.5 nm peak, with a marginal increase of 15 dB. A similar pattern is also observed in the progression of 1207.5 nm Stokes intensity following the appearance of the peak at 1238.2 nm, as shown in the third and subsidiary graphs at the bottom of Fig. 3. At output powers of 12.3 mW and 30.9 mW, the parasitic oscillations at 1238.2 nm and 1236.0 nm are observed in the spectrum, respectively, corresponding to the two inflection points (indicated by the black and blue circles in Fig. 2.) in the slope efficiency of output Stokes laser. This power clapping of Stokes laser induced by parasitic oscillations

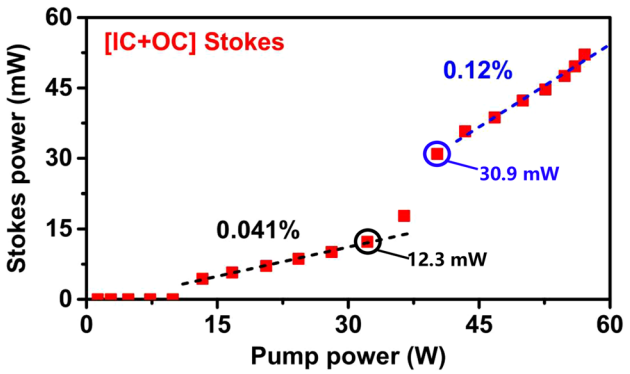

Fig. 2 Double-ended Stokes power without the insertion of LBO

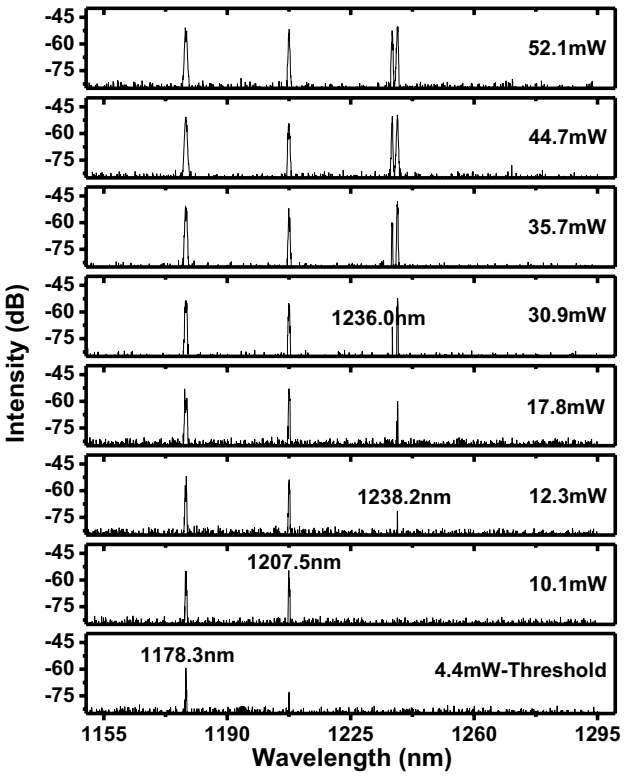

Fig. 3 Stokes spectra at different pump power without the insertion of LBO

resembles that in the cascaded Raman resonator, which has been analytically modeled in our previous work [22].

The precise power changing of each Stokes wavelength is shown in Fig. 4. 1238 nm is the second Stokes wavelength of 1178 nm at 205 cm^{-1} peak, and similar to power clamping in higher-order Stokes, when third Stokes is appearance, the power of first Stokes and third Stokes will rise. This also

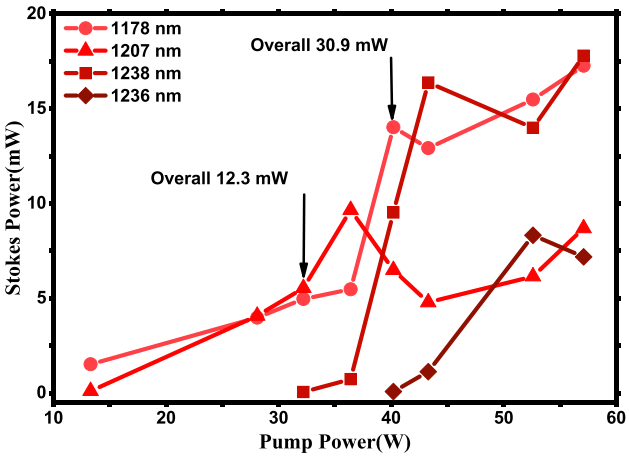

Fig. 4 Different stokes power at different pump power without the insertion of LBO

explains why the overall power slope efficiency rises when 1238 nm appears.

It is intriguing and practical to achieve multi-wavelength laser output by adjusting the phase-matching conditions of the frequency-doubling crystal LBO to facilitate interactions between different longitudinal modes in this KGW Raman cavity. As a consequence, the features of high signal-to-noise ratio visible laser output under LBO temperature tuning at maximum pump power, including the double-ended output power (S425C, Thorlabs Inc.) and spectrums (resolution of 1.5 nm, USB2000+, OceanOptics Inc.) are shown in Fig. 5. When the LBO temperature is reduced, the output wavelength of the resonator shifts progressively from yellow-green towards red, as depicted by the top photographs in Fig. 5. At temperatures of 55° C, 40.5° C, 22° C, and 24.5° C, the output laser wavelengths are primarily located at 572.6 nm, 589.1 nm, 603.8 nm, and 611.8 nm, respectively, with corresponding powers of 227 mW, 175 mW, 258 mW, and 103 mW. According to the integration calculations, the energy proportions of the center wavelengths in each spectral band are denoted as 95.99%, 94.19%, 77.76%, and 81.88%, respectively. The LBO temperature is maintained above 20° C to prevent condensation of water vapor.

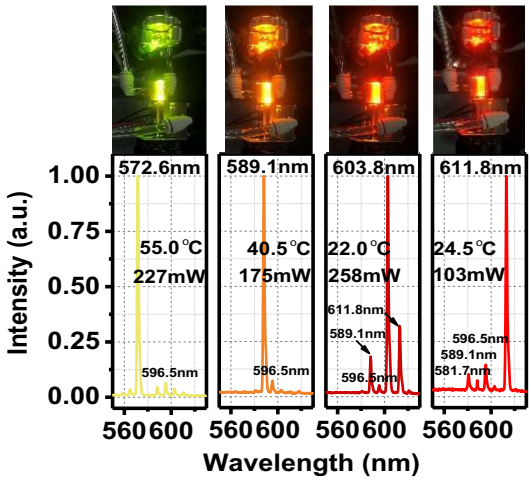

Fig. 5 Visible lasers in the yellow-red range obtained by LBO temperature tuning at maximum pump power. The photographs above show the KGW Raman resonator operating at various wavelengths in the laboratory. The error measured by the spectrometer (±1.5 nm) is corrected using the theoretical wavelength calculation

The phase-matching conditions in second-harmonic generation (SHG) and sum-frequency generation (SFG) is represented as:

$$\Delta k_{SHG} = k_{SHG} - 2k_F = 2\pi\left(n_{SHG} - n_F\right)/\lambda_{SHG} \tag{1}$$

$$\Delta k_{SHG} = k_{SHG} - k_{F_1} - k_{F_2} = 2\pi\left(n_{SFG}/\lambda_{SFG} - n_{F_1}/\lambda_{F_1} - n_{F_2}/\lambda_{F_2}\right) \tag{2}$$

where n_{SHG}, n_{SFG}, and $n_F$are the refractive indices of the SHG, SFG, and fundamental waves. The λ_{SHG}, λ_{SFG} and λ_F are the wavelengths of the SHG, SFG, and fundamental waves, respectively. The subscripts 1 and 2 in Eq. (2) corresponds to the two fundamental lasers in SFG. Based on Eqs. (1)–(2) and the Sellmeier equations [23] of LBO crystal, the temperature-dependent phase-matching conditions required for SHG/SFG for certain wavelengths can be calculated analytically by setting $\Delta k_{SHG} = 0$. The results are shown in Table 1, where the colored data are the visible wavelengths obtained in Fig. 5. Theoretically, a 596.4 nm laser can be generated by the sum frequency between 1178.3 nm and 1207.5 nm lasers when the LBO temperature is set to 31.0° C. However, this particular wavelength is not observed in Fig. 5. We attribute this to the coexistence relationship between these two lasers, as well as the significant difference in the gain coefficients between 901 cm^{-1} and 205 cm^{-1} peaks in the Ng-cut KGW crystal. The SFG between 1178.3 nm and 1236.0/1238.2 nm is expected to involve a similar mechanism, thus the observed 603.8 nm laser is anticipated to be generated through the doubling of the 1207.5 nm laser, as shown in Table 1. Based on the preceding analysis, it is reasonable to conclude that the four visible wavelengths obtained in Fig. 5. are produced by the SFG between the pump and 1236.0/1238.2 nm Stokes lasers,

Table 1 Phase-matched temperatures required for different wavelengths SHG/SFG in the LBO crystal

Physics process	Fundamental wavelength(nm)	Stokes wavelength(nm)	Generation wavelength(nm) of LBO(°C)	Theoretical temperature of LBO(°C)	Actual temperature
SFG	1065.2	1178.3	559.5	91.7	55.0
		1207.5	570.0	78.0	
		1236.0	**572.1**	**66.1**	
		1238.2	**572.6**	**65.2**	
	1178.3	1207.5	596.4	31.0	
		1236.0	603.2	23.3	
		1238.2	603.8	22.8	
	1207.5	1236.0	**610.8**	**16.2**	**24.5**
		1238.2	**611.3**	**15.8**	
SHG		1178.3	**589.2**	**40.4**	**40.5**
		1207.5	**603.8**	**22.8**	**22.0**
		1236.0	618.0	10.6	

SHG of the 1178.3 nm laser, SHG of the 1207.5 nm laser, and SFG between the 1207.5 nm and 1236.0/1238.2 nm lasers, respectively. Despite the good agreement between the experimental and theoretical LBO temperatures regarding the 589.2 nm and 603.8 nm outputs, there is a discrepancy of approximately 10° C at the wavelengths of 611.3(610.8) nm and 572.6(572.1) nm. The gap results from the limited temperature adjustment range of the LBO crystal, which is confined between 20.0° C and 55.0° C. The value of 10° C is consistent with the secondary bumps in the Sinc function curve of phase-mismatching.

Output powers of the visible lasers at 572.6 nm, 589.1 nm, 603.8 nm, and 611.8 nm (measured after OC and calculated by the considering transmittance of both IC and OC) is shown in Fig. 6. with an inset illustrating the far-field beam profile at 57 W pump. Only the beam profile of the 589.1 nm laser emission is presented here as there is little difference when the resonator operating at different wavelengths. The beam profiles at different wavelengths show negligible variation and exhibit a nearly TEM_{00} Gaussian mode without pronounced distortions that have been observed in [19], suggesting little thermal effects in the KGW crystal. The threshold of the resonator is primarily determined by cavity loss, as demonstrated by Eq. (15) in [24]. In the generation of 572.6 nm and 589.1 nm lasers, the pump and 1178.3 nm Stokes lasers are employed as the fundamental waves, leading to an increase in intracavity loss. Consequently, the thresholds (35 W) show a noticeable elevation compared to the configuration before the insertion of LBO, as illustrated by the yellow and orange curves in Fig. 6. The threshold variations for the 603.8 nm and 611.8 nm are not significant, identified as 20 W and 16.4 W in the brown and red curves.

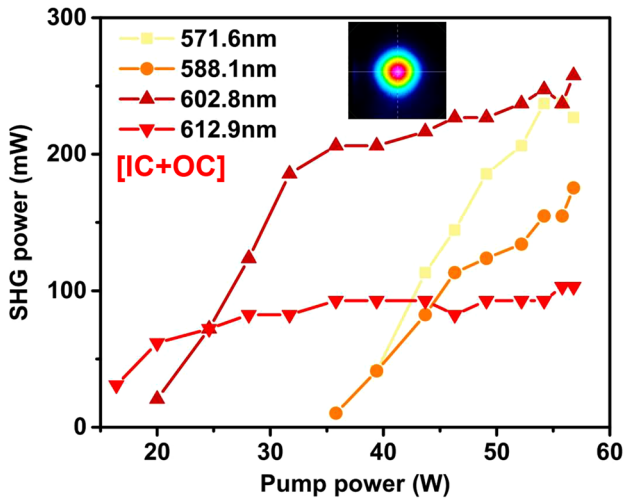

Fig. 6 Output power at wavelengths at 572.6 nm, 589.1 nm, 603.8 nm, and 611.8 nm, respectively. Inset: far-field beam profile of the 589.1 nm emission with a pump power of 57 W

Maximum powers for the visible lasers at 572.6 nm, 589.1 nm, 603.8 nm, and 611.8 nm are 227 mW, 175 mW, 258 mW, and 103 mW, respectively. Surprisingly, the LBO temperature at 572.6 nm falls on the second bump of the Sinc function, yet it still maintains a relatively high output power. This can be explained by the high power of the pump laser and the presence of the highest-order parasitic oscillation at 1236.0/1238.2 nm which enables a continuous provision of the fundamental wave power for efficient SFG. In the case of power scaling for the SHG/SFG originating from the fundamental waves being the first-order Stokes or low-order parasitic oscillations, the process of power enhancement is susceptible to generating higher-order parasitic oscillations, thereby resulting in the slope clamp. This is illustrated in the power curves of 603.8 nm and 589.1 nm, at pump powers of 31.7 W and 46.3 W, respectively. The consistently low slope of the 611.8 nm laser is mainly caused by the interdependence between the powers of the two fundamental waves and temperature-induced phase mismatching.

In this experiment, we believe that the reason for the low slope efficiency is the nonlinear intracavity losses induced by the cascade Raman process and the intracavity frequency mixing process. The cascade process and the intracavity frequency mixing will increase the resonator losses, decrease the intracavity intensity to the first Stokes laser, and thus limit the subsequent frequency conversions to the cascaded Stokes and the visible lasers. In addition, due to the low conversion efficiency, the pump power is rarely depleted and the back-reflected residual pump is emitted from the isolator. At the highest pump power of 57 W, the leaked residual pump power is about 46.6 W.

This work indicates that the Ng-cut KGW crystal is suitable for the generation of multi-wavelength visible lasers at the hundred-milliwatt level, despite the high-order parasitic oscillations resulting from limitations in cavity mirror coatings pose challenges for further power scaling. The next steps for this work include achieving higher output powers of the dual-wavelength lasers at 570 nm and 603.8 nm by adopting specific cavity mirror coatings, such as highly transmissive in the visible and 1220-1400 nm, and highly reflective in the 1000–1220 nm. Another noteworthy future of our work is realizing the watt-level single-frequency laser at 589 nm using intracavity doubling induced nonlinear loss and Raman conversion in the KGW crystal, which shows significant potential for biomedical applications with the added advantage of low cost [25–27].

4 Conclusion

To conclude, a continuous-wave wavelength-tunable laser at 572.6 nm, 589.1 nm, 603.8 nm, and 611.8 nm was demonstrated utilizing external-cavity Raman conversion in the

Ng-cut KGW crystal, combining with temperature tuning of the intracavity LBO crystal. The output powers at these four wavelengths were denoted as 227 mW, 175 mW, 258 mW, and 103 mW, respectively. Further power scaling can be achieved through the optimization of cavity mirror coatings. This concept paves the way for the development of visible wavelength tunable lasers based on a cost-effective Raman medium and provides a flexible and practical technique for air detection, optogenetics, biomedicine, and chemical analysis.

Acknowledgements This work is supported by the China Postdoctoral Science Foundation (2023M740875), the State Key Laboratory of Pulsed Power Laser Technology (SKL2022KF03), the State Key Laboratory of Quantum Optics and Quantum Optics Devices (KF202207), the Research Funds of Hangzhou Institute for Advanced Study (2023HIAS-Y005), (B02006C019019) and (2023HIAS-V004).

Author Contributions Y.Y. was in charge of research, verification and manuscript writing. Y.S. was in charge of conceptualization, methodology, review, editing and funding acquisition. X.Y. was in charge of methodology, review, editing, funding acquisition and resources. C.Z. was in charge of verification. Y.F. was in charge of resources. All authors reviewed and agreed to the published version of the manuscript.

Data availability The data that support the findings of this study are available from the corresponding author on reasonable request.

Declarations

Conflict of interest The authors declare no competing interest.

References

1. S.C. Burd, T. Leinonen, J.-P. Penttinen, D. Allcock, D.H. Slichter, R. Srinivas, A.C. Wilson, M. Guina, D. Leibfried, D. Wineland, Single-frequency 571nm VECSEL for photo-ionization of magnesium. In: Vertical External Cavity Surface Emitting Lasers (VECSELs) VI, vol. 9734, pp. 184–191 (2016). SPIE
2. X. Yang, O. Kitzler, D.J. Spence, Z. Bai, Y. Feng, R.P. Mildren, Diamond sodium guide star laser. Opt. Lett. **45**(7), 1898–1901 (2020)
3. R.G. Wheeland, Clinical uses of lasers in dermatology. Lasers Surg. Med. **16**(1), 2–23 (1995)
4. L. Huang, A. Jha, S. Shen, W.J. Chung, Visible emissions at 592 and 613 nm in Er^{3+}-Eu^{3+}-codoped tellurite fibers. Opt. Commun. **239**(4–6), 403–408 (2004)
5. E. Granados, G. Stoikos, D.T. Echarri, K. Chrysalidis, V.N. Fedosseev, C. Granados, V. Leask, B.A. Marsh, R.P. Mildren, Tunable spectral squeezers based on monolithically integrated diamond Raman resonators. Appl. Phys. Lett. **120**(15), 151101 (2022)
6. X. Yang, Z. Bai, D. Chen, W. Chen, Y. Feng, R.P. Mildren, Widely-tunable single-frequency diamond Raman laser. Opt. Express **29**(18), 29449–29457 (2021)
7. Y. Duan, J. Xu, Y. Wei, X. Jin, Z. Li, H. Zhu, Yellow-orange wavelength-switchable laser emission generated from c-cut Nd: YVO_4 self-Raman with 890 and 259 cm^{-1} shifts. J. Lumin. **267**, 120402 (2024)
8. C.-L. Hsieh, H.-J. Huang, C.-L. Chen, H.-C. Liang, Y.-F. Chen, Selectable two-wavelength Nd: YVO_4 raman laser at 671 and 714 nm. Opt. Lett. **48**(6), 1510–1513 (2023)
9. J. Jakutis-Neto, J. Lin, N.U. Wetter, H. Pask, Continuous-wave watt-level Nd: YLF/KGW Raman laser operating at near-ir, yellow and lime-green wavelengths. Opt. Express **20**(9), 9841–9850 (2012)
10. Y. Chen, D. Li, Y. Lee, C. Lee, H. Huang, C. Tsou, H. Liang, Highly efficient solid-state Raman yellow-orange lasers created by enhancing the cavity reflectivity. Opt. Lett. **46**(4), 797–800 (2021)
11. R.P. Mildren, H. Ogilvy, J.A. Piper, Solid-state Raman laser generating discretely tunable ultraviolet between 266 and 320 nm. Opt. Lett. **32**(7), 814–816 (2007)
12. J. Guo, H. Zhu, S. Chen, X. Xu, Y. Duan, C. Xu, D. Tang, Yellow, lime and green emission selectable by bbo angle tuning in Q-switched Nd: YVO_4 self- Raman laser. Laser Phys. Lett. **15**(7), 075803 (2018)
13. L. Zhang, Y. Duan, Y. Sun, Y. Chen, Z. Li, H. Zhu, G. Zhang, D. Tang, Passively Q-switched multiple visible wavelengths switchable YVO_4 Raman laser. J. Lumin. **228**, 117650 (2020)
14. Y. Duan, Y. Sun, H. Zhu, T. Mao, L. Zhang, X. Chen, Yvo 4 cascaded Raman laser for five-visible-wavelength switchable emission. Opt. Lett. **45**(9), 2564–2567 (2020)
15. Y. Duan, H. Zhu, G. Zhang, D. Tang, Multiple visible wavelength switchable cascaded self-raman laser based on selective wave-mixing mechanism. Appl. Phys. Lett. **123**(26), (2023)
16. R. Casula, J.-P. Penttinen, M. Guina, A.J. Kemp, J.E. Hastie, Cascaded crystalline Raman lasers for extended wavelength coverage: continuous-wave, third-stokes operation. Optica **5**(11), 1406–1413 (2018)
17. Q. Sheng, J. Geng, T. Liu, S. Fu, W. Shi, J. Yao, A continuous-wave Nd: YVO_4-KGW intracavity Raman laser with over 34% diode-to-stokes optical efficiency. High Power Laser Sci. Eng. **12**, 19 (2024)
18. A. McKay, O. Kitzler, R.P. Mildren, Thermal lens evolution and compensation in a high power KGW Raman laser. Opt. Express **22**(6), 6707–6718 (2014)
19. A. McKay, O. Kitzler, R.P. Mildren, High power tungstate-crystal Raman laser operating in the strong thermal lensing regime. Opt. Express **22**(1), 707–715 (2014)
20. D.J. Spence, Spectral effects of stimulated Raman scattering in crystals. Prog. Quantum Electron. **51**, 1–45 (2017)
21. Y. Sun, M. Li, R.P. Mildren, Z. Bai, H. Zhang, J. Lu, Y. Feng, X. Yang, High-power continuous-wave single-frequency diamond Raman laser at 1178 nm. Appl. Phys. Lett. **121**(14), (2022)
22. M. Li, O. Kitzler, R.P. Mildren, D.J. Spence, Modelling and characterisation of continuous wave resonantly pumped diamond Raman lasers. Opt. Express **29**(12), 18427–18436 (2021)
23. K. Kato, Temperature-tuned 90 ° phase-matching properties of LiB_3O_5. IEEE J. Quantum Electron. **30**(12), 2950–2952 (1994)
24. O. Kitzler, A. McKay, D.J. Spence, R.P. Mildren, Modelling and optimization of continuous-wave external cavity Raman lasers. Opt. Express **23**(7), 8590–8602 (2015)
25. N. Fauzi, N. Suardi, M.Z. Mustafa, A.A. Rahman, Biostimulation study of ATP content on anaemic human blood cell induced by 589 nm low level laser. In: AIP Conference Proceedings, vol. 2016 (2018). AIP Publishing
26. E.L. Tanzi, J.R. Lupton, T.S. Alster, Lasers in dermatology: four decades of progress. J. Am. Acad. Dermatol. **49**(1), 1–34 (2003)
27. S. Kaiplavil, Thin photothermal endoscope for biomedical applications. J. Biomed. Opt. **18**(9), 097008 (2013)